

This work was written as part of one of the author's official duties as an Employee of the United States Government and is therefore a work of the United States Government. In accordance with 17 U.S.C. 105, no copyright protection is available for such works under U.S. Law.

Public Domain Mark 1.0

<https://creativecommons.org/publicdomain/mark/1.0/>

Access to this work was provided by the University of Maryland, Baltimore County (UMBC) ScholarWorks@UMBC digital repository on the Maryland Shared Open Access (MD-SOAR) platform.

**Please provide feedback**

Please support the ScholarWorks@UMBC repository by emailing [scholarworks-group@umbc.edu](mailto:scholarworks-group@umbc.edu) and telling us what having access to this work means to you and why it's important to you. Thank you.

## Bio-optics of the Chesapeake Bay from measurements and radiative transfer closure

Maria Tzortziou <sup>a,\*</sup>, Jay R. Herman <sup>b</sup>, Charles L. Gallegos <sup>c</sup>, Patrick J. Neale <sup>c</sup>,  
Ajit Subramaniam <sup>d</sup>, Lawrence W. Harding Jr. <sup>e</sup>, Ziauddin Ahmad <sup>f</sup>

<sup>a</sup> University of Maryland, Earth System Science Interdisciplinary Center, College Park, MD 20742, USA

<sup>b</sup> NASA/Goddard Space Flight Center, Greenbelt, MD 20771, USA

<sup>c</sup> Smithsonian Environmental Research Center, Edgewater, MD 21037, USA

<sup>d</sup> Lamont Doherty Earth Observatory, Columbia University, Palisades, NY 10964, USA

<sup>e</sup> University of Maryland Center for Environmental Science, Horn Point Laboratory, Cambridge, MD 21613, USA

<sup>f</sup> Science and Data Systems, Inc., Silver Spring, MD 20906, USA

Received 12 July 2005; accepted 17 February 2006

Available online 18 April 2006

### Abstract

We combined detailed bio-optical measurements and radiative transfer modeling to perform an ‘optical closure’ experiment for an optically complex and biologically productive region of the Chesapeake Bay. We used this experiment to evaluate certain assumptions commonly used in bio-optical models, and to investigate which optical characteristics are most important to accurately model and interpret remote sensing ocean-color observations in these Case 2 waters. Direct measurements were made of the magnitude, variability, and spectral characteristics of backscattering and absorption that are critical for accurate parameterizations in satellite bio-optical algorithms and underwater radiative transfer simulations. We found that the ratio of backscattering to total scattering (i.e. the backscattering fraction,  $b_b/b$ ) varied considerably depending on particulate loading, distance from land, and mixing processes, and had an average value of 0.0128 at 530 nm. Incorporating information on the magnitude, variability, and spectral characteristics of particulate backscattering into the radiative transfer model, rather than using a volume scattering function commonly assumed for turbid waters, was critical to obtaining agreement between model calculations and measured radiometric quantities. In-situ measurements of absorption coefficients need to be corrected for systematic overestimation due to scattering errors, and this correction commonly employs the assumption that absorption by particulate matter at near-infrared wavelengths is zero. Direct measurements, however, showed that particulate matter in the Bay had small, but non-zero, absorption in the 700–730 nm wavelength region. Accounting for this residual particulate absorption when correcting in-situ measured absorption spectra for scattering errors was important in model simulations of water reflectance in the green wavelengths, where reflectance spectra in estuarine waters peak. Sun-induced chlorophyll fluorescence considerably affected the magnitude of water reflectance in the red wavelengths. Very good optical closure was obtained between independently measured water inherent optical properties and radiation fields, after applying the results from our detailed measurements to model bio-optical processes in these Case 2 waters. The good optical closure was consistent over the observed wide range of water optical characteristics. Average absolute percent differences between measured and model-estimated water-leaving radiances were 6.35% at 443 nm, 7.73% at 554 nm, and 6.86% at 670 nm, considerably smaller than those presented in the few studies of optical closure performed previously in near shore waters of similar optical complexity. These results show that bio-optical processes can be confidently modeled in complex estuarine waters, and underscore the importance of accurate formulations for backscattering, long-wavelength particulate absorption, and chlorophyll fluorescence. © 2006 Elsevier Ltd. All rights reserved.

**Keywords:** estuaries; coastal waters; backscattering; chlorophyll fluorescence; particulate absorption; remote sensing

\* Corresponding author.

E-mail address: [martz@code613-3.gsfc.nasa.gov](mailto:martz@code613-3.gsfc.nasa.gov) (M. Tzortziou).

## 1. Introduction

Remote sensing of ocean color is based on measurements of light that leaves the water surface and reaches an aircraft or satellite-borne sensor, carrying with it information about the water optical characteristics. High concentrations of optically significant, non-covarying, biogeochemical constituents, such as phytoplankton, colored dissolved organic matter (CDOM), and non-algal particles, influence ocean color in estuarine and coastal regions. In order to use remote sensing to estimate changes in coastal water composition and biological activity it is necessary to develop appropriate, and in many cases ‘regionally-specific’, bio-optical algorithms relating the remotely sensed water reflectance to the optical properties (i.e. absorption and scattering) of the individual water constituents (e.g. Garver and Siegel, 1997; Carder et al., 1999; Maritorena et al., 2002). However, for many estuarine and coastal waters certain optical properties (e.g. particulate backscattering) remain poorly characterized (e.g. Babin et al., 2003; Magnuson et al., 2004). Therefore, specific, in-situ data on how these properties affect water reflectance in the visible are needed for effective interpretation of remotely sensed ocean color in near shore regions.

Development of effective coastal bio-optical algorithms and validation of remote sensing observations using in-situ bio-optical data require testing the accuracy of the data and the consistency, or ‘optical closure’, among the independently measured quantities. Demonstration of optical closure involves solution of the equations of radiative transfer using measured boundary conditions (e.g. incident radiance) and inherent optical properties (IOPs) to predict apparent optical properties, such as downwelling irradiance ( $E_d(\lambda, z)$ ), or remote sensing reflectance ( $R_{rs}(\lambda)$ ). Closure is obtained to the extent that predictions match independent measurements. Radiative transfer modeling can be used to investigate errors in measurement methodology and uncertainties in relationships used in bio-optical models, as well as examine the relative importance of several bio-optical properties in determining coastal ocean color (schematic illustration shown in Fig. 1). However, very few studies have been published on optical closure for optically complex near shore waters (e.g. Bulgarelli et al., 2003; Chang et al., 2003).

Three bio-optical properties, for which in-situ determinations remain scarce, are particularly important to effective interpretation of coastal ocean color: (1) variability in particulate backscattering,  $b_b$ , and the ratio of backscattering to total scattering by particles, i.e. backscattering fraction,  $b_b/b$  (e.g. Mobley et al., 2002); (2) long-wavelength non-algal particulate absorption characteristics (e.g. Babin and Stramski, 2002; Tassan and Ferrari, 2003); and (3) contribution of solar-induced chlorophyll fluorescence to remotely sensed water reflectance (e.g. Gower, 1980; Maritorena et al., 2000). The  $R_{rs}$ , defined by the ratio of water-leaving radiance,  $L_w$ , to downwelling surface irradiance,  $E_s$ , is to a first approximation proportional to the ratio of backscattering to absorption,  $b_b/a$  (e.g. Morel and Prieur, 1977). Thus, both backscattering and absorption are important in determining the magnitude and spectral shape of water reflectance. However, information on particulate backscattering magnitude, spectral shape, or angular dependence is scarce for estuarine and coastal waters. As a result, modeling of backscattering processes has been largely based on a few existing data sets and assumptions regarding  $b_b/b$  variability. For example, the Petzold ‘average particle’ volume scattering function (VSF) (Petzold, 1972), derived from three measurements of VSF in San Diego Harbor and with an estimated  $b_b/b$  of 0.018, has been widely assumed for modeling  $b_b$  in coastal areas. The lack of direct measurements of  $b_b$  poses a significant limitation in the development of appropriate backscattering parameterizations for coastal satellite algorithms, or the evaluation of remote sensing backscattering products (e.g. Magnuson et al., 2004). Water absorption properties are more frequently measured as part of near shore water-quality studies. In-situ measurements of dissolved and particulate absorption have been made in estuarine and coastal waters by several ship-based monitoring programs during the last decades (e.g. Tassan, 1988; Carder et al., 1989; Roesler et al., 1989; Magnuson et al., 2004). However, current understanding of variations in the non-algal particulate absorption spectra is still limited (Babin et al., 2003) and uncertainties remain about the long-wavelength particulate absorption in highly turbid waters. When using in-situ measurements of total absorption for radiative transfer modeling in coastal waters, small errors at

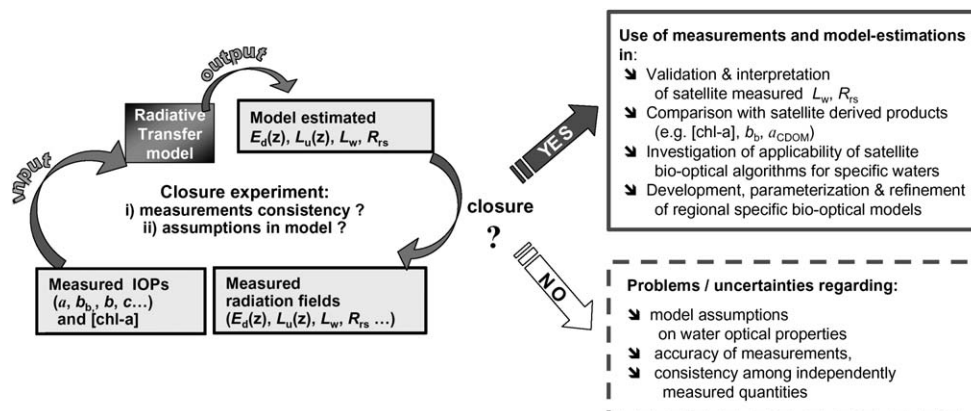


Fig. 1. ‘Optical closure’ and its role in the interpretation of coastal ocean color.

green wavelengths, where the absorption spectrum has a broad minimum, can amplify errors in estimation of  $R_{rs}$ . Ramifications of assuming zero particulate absorption at near-infrared wavelengths when correcting in-situ absorption measurements at green wavelengths for scattering bias (e.g. Zaneveld et al., 1994) have not been explored. Sun-induced chlorophyll fluorescence affects the magnitude and spectral shape of reflectance in natural waters (e.g. Gordon, 1979; Maritorena et al., 2000). The remotely sensed chlorophyll fluorescence signal can be strong in estuaries like the Chesapeake Bay that are characterized by high chlorophyll concentrations. Optical closure studies provide a means of evaluating the effect of chlorophyll fluorescence on  $R_{rs}$  and, consequently, a basis for remote sensing retrieval of chlorophyll.

Chesapeake Bay is a large and biologically productive estuary characterized by Case 2 waters with strong backscattering and absorption (e.g. Tzortziou, 2004; Harding et al., 2005). Remote sensing is a potentially powerful tool for studying phytoplankton dynamics and managing water quality in the Chesapeake Bay by virtue of its ability to resolve steep spatial gradients and temporal variability in optically significant constituents (Harding et al., 2005). However, riverine inputs of dissolved and particulate matter and independent variation among the bio-optically significant constituents in these waters, mean that each of the three factors listed above complicates successful retrieval of key properties from remote sensing (Magnuson et al., 2004). An approach combining new in-situ measurements of particulate backscattering and absorption with radiative transfer modeling in Chesapeake Bay is needed to resolve the difficulties imposed by the optical complexities.

In this paper we present an analysis of in-situ, bio-optical measurements from a region of the Chesapeake Bay, including direct measurements of the magnitude, variability and spectral characteristics of particulate backscattering and absorption. We then apply our measurements to model simulations of underwater radiation fields using the Hydrolight code (Mobley, 1988). Our main objective was to use a combination of detailed bio-optical data with radiative transfer closure results to evaluate: (1) alternative formulations for the backscattering processes in these waters, and the importance of accurate representation of  $b_b$  in radiative transfer calculations; (2) long-wavelength particulate absorption and its effect, as well as that of chlorophyll fluorescence, on model simulations of  $R_{rs}$  spectra; (3) the consistency and optical closure among independently measured IOPs and radiometric quantities, as a step towards applying these data to the interpretation of satellite observations and the investigation of bio-optical relationships for improved remote sensing retrievals in these Case 2 waters.

## 2. Material and methods

### 2.1. Location and duration of measurements

Measurements of IOPs and water quality were made at four stations in the Chesapeake Bay designated: Poplar Island (PI),

Herring Bay (HB), Tilghman Island (TI) and Jetta (JT) (38.71°–38.89°N latitude, 76.34°–76.54°W longitude) (Fig. 2). These stations were located in the mesohaline region of the upper Bay, and included sites in both lateral and mid-channel waters. Measurements were made during 17 cruises performed between June 2001 and November 2002.

### 2.2. In-situ measurements and calculations

Vertical profiles of total (minus pure water) attenuation,  $c_{t-w}(\lambda, z)$ , and absorption,  $a_{t-w}(\lambda, z)$ , were measured at nine wavelengths (412–715 nm) using a WETLabs AC-9. Measurements were corrected for the temperature and salinity dependence of absorption by pure water (Pegau et al., 1997) using temperature and salinity data measured with Hydrolab Datasonde 4a. Particulate scattering,  $b_p(\lambda, z)$ , was estimated as the difference between  $c_{t-w}(\lambda, z)$  and  $a_{t-w}(\lambda, z)$ , after applying additional corrections to account for scattering losses manifested as overestimates of measured absorption (Kirk, 1992). We initially corrected the AC9 measurements for scattering errors according to Zaneveld et al. (1994). This correction is based on the assumption that the sum of particulate and dissolved absorption at 715 nm is zero. The correction is applied by subtracting a fraction of the AC9 measured scattering from the whole measured absorption spectrum. The fraction is scaled to set non-water absorption at 715 nm to zero. That is,

$$a_{t-w}(\lambda)_{\text{corrected}} = a_{t-w}(\lambda)_{\text{measured}} - \frac{a_{t-w}(715)_{\text{measured}}}{b_p(715)_{\text{measured}}} b_p(\lambda)_{\text{measured}} \quad (1)$$

Based on two lines of evidence in our results (see below, Sections 3 and 4), we modified this correction to allow for non-zero particulate absorption at 715 nm.

An ECOVSF3 instrument (WetLabs Inc; Moore et al., 2000) was used to measure scattering at three backscattering angles (100°, 125°, 150°) and three visible wavelengths (450, 530, 650 nm). Measurements were corrected for attenuation and were integrated (90–180°) to obtain total  $b_b$  according to manufacturer's instructions. Measurements by Boss et al. (2004) in the Case 2 waters off the coast of New Jersey showed that estimates of  $b_b$  using an ECOVSF were within 1.5% ( $R^2 = 0.99$ ) of the  $b_b$  measurements made using an HOBILabs Hydrosat-6 (Maffione and Dana, 1997). These results increase confidence in the accuracy of the backscattering measurements technique, especially since the instruments have large differences in design and calibration (Boss et al., 2004). ECOVSF3 measures  $b_b$  only at wavelengths 450, 530, and 650 nm. As there are not enough data in the literature on the spectral dependence of  $b_b$  in the UV and near-infrared wavelengths for Chesapeake Bay, we extrapolated  $b_b$  as a constant at wavelengths shorter than 450 nm and longer than 650 nm in our radiative transfer modeling.

Two sensor arrays were used to measure underwater radiation fields, depending on instrument availability. On eight cruises underwater upwelling,  $E_u(z)$ , and downwelling,  $E_d(z)$ , spectral irradiance profiles, and above-water surface

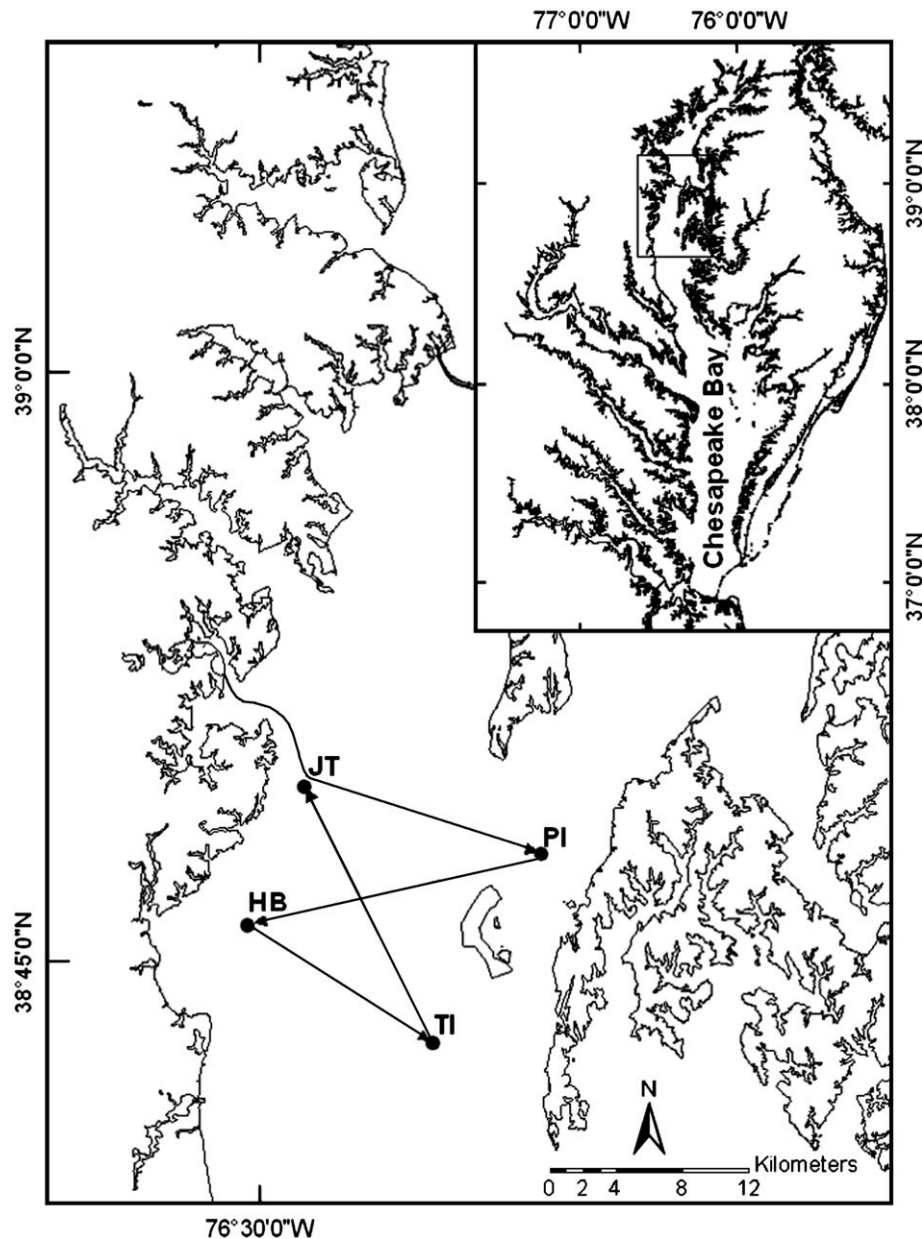


Fig. 2. Location of in-situ measurements (stations HB, PI, TI and JT) and cruise track. The starting point was the SERC dock located in the Rhode River sub-estuary, along the western shore of the Chesapeake Bay.

downwelling irradiance,  $E_s$ , were measured using Satlantic OCI-200 seven-channel (412–684 nm) irradiance sensors. The sensors were mounted on a custom frame so that up- and downwelling sensors were nearly coplanar. On the rest of our cruises we used a Satlantic MicroPro free-falling radiometer to measure water column profiles of upwelling radiance,  $L_u(z)$ , and  $E_d(z)$ , and Satlantic OCR-507 Surface Reference Irradiance sensors for measurements of  $E_s$ , in 14 wavebands (400–700 nm). The MicroPro contains a pressure sensor that gives depth, and a miniature biaxial clinometer for tilt measurements (accuracy of  $0.2^\circ$ ) (Satlantic MicroPro Operation Manual, 2002). Results from three casts were averaged, except that measurements not meeting quality control (e.g. casts characterized by large tilt-angles or changing

cloudiness conditions) were omitted from analysis. A correction was applied to the radiometric measurements through the instrument's calibration for the immersion effect (Satlantic MicroPro Operation Manual, 2002). Measurements of  $L_u(z)$  were corrected for the depth offset between the  $E_d$  and  $L_u$  sensors, and for self-shading (Gordon and Ding, 1992; Zibordi and Ferrari, 1995). According to Gordon and Ding (1992) and Zibordi and Ferrari (1995), the magnitude of instrument self-shading error depends mainly on the size of the radiometer, the solar zenith angle, and the total in-water absorption, and can be very significant in highly absorbing, coastal waters. However, field observations by Zibordi and Ferrari (1995) suggest that the presence of highly scattering material, as occurs in Chesapeake Bay, could reduce the self-shading error below



that theoretically predicted based on the Gordon and Ding model. The MicroPro instrument, used in our measurements of  $L_u(z)$ , has a smaller diameter (6.4 cm) compared to other radiometric instruments and is less subject to instrument self-shading (Harding and Magnuson, 2002).

To estimate  $L_w$ , we extrapolated underwater  $L_u(z)$  measurements to just below the water surface  $z = 0^-$  and estimated transmittance through the water–air interface. The upwelling radiance just below the water surface,  $L_u(0^-, \lambda)$  was estimated through non-linear least squares fitting (Sigma-Stat software) of measured  $L_u(z, \lambda)$  to the equation  $L_u(z, \lambda) = L_u(0^-, \lambda) \exp(-K_{L_u} z)$ , where  $K_{L_u}$  is the diffuse attenuation coefficient for the upwelling radiance, to a good approximation constant in the layer 0–3 m used in the regressions for the cases studied here. The coefficients of determination ( $R^2$  values) for the non-linear exponential fits were in most cases better than 0.99. To estimate  $L_w$ ,  $L_u(0^-, \lambda)$  was propagated through the water–air interface:

$$L_w(\lambda, \theta, \varphi) = L_u(0^-, \lambda, \theta', \varphi) \frac{(1 - r(\theta', \theta))}{n_w^2} \quad (2)$$

where  $\theta'$  is the direction of the upward traveling photons incident from the water body onto the water surface,  $\theta$  is the direction of the transmitted photons,  $r(\theta', \theta)$  is the Fresnel reflectance for the associated directions  $\theta'$  and  $\theta$ , and  $n_w$  is the index of refraction of water ( $n_w \approx 1.34$ ) (Mobley, 1994). For the geometry of our measurements, the zenith angle of water-leaving radiance and the nadir angle of in-water upward radiance are zero ( $\theta' = \theta = 0$ ) and the transmittance is  $(1 - r(\theta', \theta)) \approx 0.98$ . Therefore,  $L_w(\lambda)$  can be estimated from Eq. (2), as:

$$L_w(\lambda) = 0.544 L_u(0^-, \lambda).$$

### 2.3. Laboratory measurements

Water samples were collected from discrete depths at the four stations for analysis of IOPs and water quality. We used filtration to partition absorption among particulate and dissolved components. Particulate material was collected on 25 mm glass fiber filters (Whatman GF/F), while the filtrate passing a 0.22  $\mu\text{m}$  pore-diameter polycarbonate membrane filter was used to measure CDOM absorption. Absorbance spectra were measured using a Cary-IV dual-beam spectrophotometer to estimate the contribution of phytoplankton, non-algal particulate matter, and CDOM to total light absorption, using the approach of Gallegos and Neale (2002). Absorption spectral slope coefficients describing the exponential decrease of absorption with increasing wavelength for CDOM,  $S_{\text{CDOM}}$ , and non-algal particulate matter,  $S_{\text{nap}}$ , were determined by applying non-linear exponential fits to the absorption coefficients vs wavelength (290–750 nm). Absorbance spectra of the filters were corrected for scattering errors using a path-length amplification factor estimated empirically by comparing particulate optical density measured on filters and in particle suspension (Mitchell et al., 2000).

Measurements of the optical density of the particle suspension were made using the Cary-IV equipped with a 110 mm integrating sphere coated with polytetrafluoroethylene, by placing the sample at the center of the sphere to minimize scattering errors (Nelson and Prezelin, 1993; Babin and Stramski, 2002). Chlorophyll-*a* concentration, [chl-*a*], was measured spectrophotometrically on 90% acetone extracts of seston collected on 47 mm GF/F glass fiber filters (Jeffrey and Humphrey, 1975).

### 2.4. Radiative transfer modeling

We used the extensively validated Hydrolight underwater radiative transfer program (Mobley, 1988) to estimate water-leaving radiances and underwater radiation fields for the Chesapeake Bay. These calculations allowed us to examine the consistency between independently measured bio-optical quantities, for those cruises when detailed measurements of in-water IOPs, upwelling radiances, and downwelling irradiances (MicroPro measurements) were available. Mobley (1994) has given a detailed description of the physical assumptions and mathematical calculations in the Hydrolight model.

The measured quantities used as inputs to perform model calculations included: (1)  $E_s(\lambda)$  spectra; (2) vertical profiles of  $a_{t-w}(\lambda, z)$ ,  $c_{t-w}(\lambda, z)$ , and  $b_b$ ; (3) observations of surface wind-speed for model estimations of water surface roughness (Cox and Munk, 1954; Mobley, 2002); (4) observations of cloudiness during in-situ measurements; (5) solar zenith angle estimations based on the exact time and location of the measurements. The Pope and Fry (1997) absorption values for pure water and the seawater scattering coefficients of Morel (1974) as retabulated by Smith and Baker (1981) were used in our model simulations. As the water at the four measurement sites in the Chesapeake Bay was quite turbid, and information on bottom reflectance was not available, the water column was assumed to be infinitely deep below the greatest depth of interest. Sensitivity studies in which we varied the bottom reflectance in the model showed that this assumption did not affect model estimates of water-leaving radiances (Tzortziou, 2004).

Raman scattering and CDOM and chlorophyll-*a* fluorescence were included in all model runs, except as indicated. Measurements of [chl-*a*] and CDOM absorption were used as inputs in model simulations of chlorophyll and CDOM fluorescence. Model runs were performed over a 350–700 nm wavelength range to include the relevant fluorescence excitation and emission wavelengths (Mobley and Sundman, 2000). Measurements of fluorescence quantum yield were not performed in this study. Therefore, we used Hydrolight default assumptions for fluorescence efficiency and wavelength redistribution functions for fluorescence by chlorophyll (Mobley, 1994) and CDOM (Hawes, 1992).

We varied the option selected to represent backscattering within Hydrolight as part of our investigation. The widely used “Petzold average particle” VSF, with a backscattering fraction of 0.018, is available as a tabulated function within Hydrolight. We compared predictions using the Petzold

average particle VSF with those using the more versatile Fournier-Forand (FF) phase function, also available as an option within Hydrolight (Mobley et al., 2002). The FF phase function is an analytical representation of the angular scattering of light that is determined by the particle index of refraction and the particle-size distribution (Fournier and Forand, 1994). Mobley et al. (2002) demonstrated that the FF phase function can be specified mainly by the backscattering fraction,  $b_b/b$ , which we determined from our in-situ measurements using the AC9 and ECOVSF3 instruments.

### 3. Results

A wide range of in-water optical characteristics, atmospheric, and air–water surface boundary conditions were observed in the Chesapeake Bay during our cruises (e.g. Table 1). The large variation in measured IOPs and  $E_s$  resulted in large spatial and temporal variations in the magnitude of measured water-leaving radiance,  $L_w$  (results presented in following sections). However, in all cases, maximum values of  $L_w$  occurred in the green wavelengths because of the high CDOM and non-algal particulate absorption in the blue and the high pure-water absorption in the red region of the spectrum.

Radiative transfer modeling was compared with measured bio-optical quantities for a total of 16 profiles. Almost 85% of the IOP and [chl-*a*] values observed in the Chesapeake Bay during all our cruises were within the range of values for which model simulations were performed (Table 1). We selected an example data set obtained at station PI on 28 September 2001 for the purpose of comparing measurements and model calculations of  $E_d$ ,  $L_u$ , and  $L_w$  in the next sections.

#### 3.1. Backscattering properties

In-situ measurements of backscattering showed considerable variability, depending on particulate loading, distance from land, and mixing processes. Surface  $b_b$  at 530 nm ranged from 0.013 to 0.166  $m^{-1}$ . Higher  $b_b$  values (by more than a factor of two in some cases) were observed consistently in the turbid water near station JT. Considerable variation was also observed in the estimated backscattering fraction with  $b_b/b$  at 530 nm ranging from 0.006 to 0.036. Large values were measured close to the bottom, consistent with an increase in the proportion of resuspended inorganic sediments relative to organic particles with depth. Particulate  $b_b/b$  at 530 nm had an average value of  $0.0128 \pm 0.0032$  (s.d.), considerably

smaller than the Petzold average particle  $b_b/b$  of 0.018. Spectral dependence of  $b_b/b$  was weak, with average  $b_b/b$  equal to  $0.0133 \pm 0.0032$  at 450 nm and  $0.0106 \pm 0.0029$  at 650 nm.

We investigated the effect of the choice of VSF and the importance of variability in  $b_b$  magnitude and spectral shape for accurate modeling of  $E_d(z)$ ,  $L_u(z)$ , and  $L_w$ , using the example data set (measured  $b_b/b$  in the blue–green close to 0.015) (Fig. 3, open diamonds). Assumption of a Petzold phase function in our model simulations led to an underestimation of  $E_d$  by  $\sim 20\%$  at 3–5 m depths compared to measurements.  $L_w$  was overestimated by 30% in the blue wavelengths and by 30–50% in the 550–650 nm wavelength region (Fig. 3, stars). This large disagreement resulted mainly because the assumed  $b_b/b$  of 0.018 was too large for the specific waters.

The agreement between model simulations and measurements markedly improved when we incorporated information on  $b_b/b$  magnitude into the model by using a Fournier-Forand (FF) phase function scaled to measured  $b_b/b$  profiles (Mobley et al., 2002). Use of an FF phase function with a backscattering fraction constant with wavelength and depth ( $b_b/b = 0.015$ ) resulted in an overestimation of  $L_w$  by  $\sim 15\%$  in the blue–green wavelengths (compared to  $\sim 30\%$  when using the Petzold assumption) because the measured  $b_b/b$  was close to 0.015 at this wavelength region. Overestimates were larger, ca. 20–30% at the red wavelengths because measured  $b_b/b$  showed a small decrease with increasing wavelength (Fig. 3, filled circles).

Finally, modeling  $b_b$  using an FF phase function and accounting for the  $b_b/b$  spectral shape and vertical structure further improved the agreement between data and model simulations. Absolute percent differences between model-estimated and measured  $L_w(\lambda)$  were reduced to less than 10% at all wavebands (Fig. 3, filled squares). Indeed, use of FF

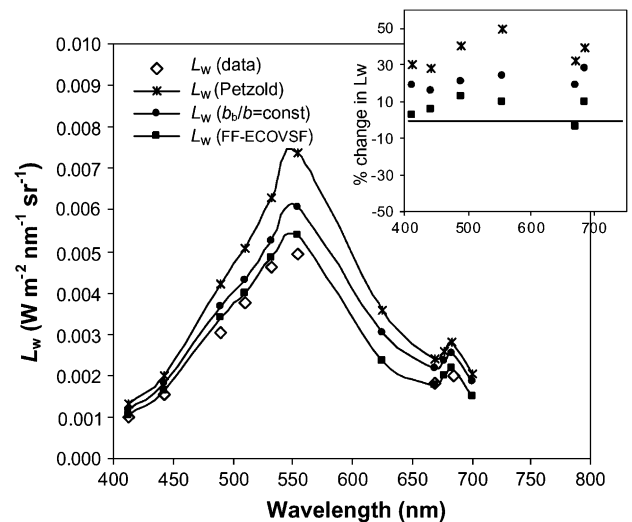


Fig. 3.  $L_w$  spectra estimated using: (1) a Petzold “average particle” scattering phase function (stars), (2) an FF scattering phase function with a constant backscattering ratio,  $b_b/b = 0.015$  (filled circles); and (3) an FF scattering phase function as determined by measured wavelength- and depth-dependent  $b_b/b$  (filled squares). Measured  $L_w$  are shown as open diamonds. Percent differences in  $L_w$  between measurements and model estimations are shown in the inset figure (percent differences estimated as  $(L_{w(model)} - L_{w(data)})/L_{w(data)}$ ).

Table 1

Range of values (min–max) of IOPs for those days for which Hydrolight simulations were performed. These span about 85% of observed values during all 17 cruises in the Chesapeake Bay waters

	$a_{t-w}(440)$ ( $m^{-1}$ )	$a_{t-w}(676)$ ( $m^{-1}$ )	$c_{t-w}(440)$ ( $m^{-1}$ )	$c_{t-w}(676)$ ( $m^{-1}$ )	$b_b/b$ (530)	[chl- <i>a</i> ] ( $mg\ m^{-3}$ )
Min	0.6	0.12	2.5	1.6	0.006	4.8
Max	1.44	0.44	8.5	6.3	0.020	23

phase function constrained by measured wavelength- and depth-dependent  $b_p/b$  consistently improved agreement between model and data for all our cruises. However, we observed a remaining tendency for the model to overestimate both  $L_u$  and  $E_d$  profiles, especially for the green wavelengths. We, therefore, considered whether systematic underestimation of absorption could be responsible for this tendency toward overestimation at green wavelengths.

### 3.2. Absorption properties

Dissolved material and non-algal particles contributed considerably to total light absorption in the short visible wavelengths. Their combined contribution to  $a_{t-w}$  was on average 59% at 488 nm, and even larger at shorter wavelengths due to the exponential increase in absorption of both substances with decreasing wavelength.  $S_{CDOM}$  had an average value of  $0.018 \text{ nm}^{-1}$ , whereas average  $S_{nap}$  was  $0.011 \text{ nm}^{-1}$ . An absorption spectral slope of  $0.011 \text{ nm}^{-1}$  for non-algal particles implies that non-algal particulate absorption at 715 nm would be nearly 5% of its value at 440 nm. Measurements of particulate absorption spectra both for particulates on glass fiber filters (standard method) and for particle suspensions inside an integrating sphere showed low, but non-zero, absorption in the wavelength region 700–730 nm (example data shown in Fig. 4). Measured  $a_{t-w}(715)$  values for the studied region of the Bay were typically  $0.03 \text{ m}^{-1}$  ( $\pm 0.01$  s.d.), commensurate with expectations based on  $S_{nap}$ .

Ramifications of this residual, long-wavelength, particulate absorption for estimation of radiometric quantities in the visible were examined more thoroughly for the example data set (Fig. 5). For this case measured particulate absorption at 715 nm was close to  $0.02 \text{ m}^{-1}$  (Fig. 4). Large differences

between measured and model-estimated  $L_u$  and  $E_d$  profiles were observed at the green wavelengths (Fig. 5, open circles) when model simulations were performed using as inputs AC9 data corrected assuming zero  $a_{t-w}(715)$  (Eq. (1)). Percent differences between model-estimated and measured  $L_u$  values at 1 m depth were 17% at 490 nm and 17.2% at 554 nm. The model overestimated both  $E_d(z)$  and  $L_u(z)$ , and the disagreement between measurements and model estimations increased with increasing depth. Similar results were observed when comparing measurements and model estimations for other days and stations. The overestimation of both  $L_u$  and  $E_d$  by the model could not be explained only by errors in measured  $b_p$ , as overestimation, for example, of  $b_p$  would result in overestimation of  $L_u$  but underestimation of  $E_d$ .

When we ran the model allowing for non-zero particulate absorption at 715 nm when correcting in-situ measured absorption spectra, the agreement between measurements and model results was considerably improved for both  $L_u$  and  $E_d$  (Fig. 5, filled circles). In this case, a modified AC9 data correction for scattering errors was performed according to:

$$a_{t-w}(\lambda)_{\text{corrected}} = a_{t-w}(\lambda)_{\text{measured}} - \frac{a_{t-w}(715)_{\text{measured}} - a_{\text{CARY}}(715)}{b_p(715)_{\text{measured}}} \times b_p(\lambda)_{\text{measured}} \quad (3)$$

where  $a_{\text{CARY}}(715)$  is the total (minus pure water) absorption at 715 nm measured spectrophotometrically. Accounting for the residual particulate absorption at 715 nm had relatively larger effects on model estimates of radiation fields in the green wavelength region (where total absorption is relatively small), while changes in the blue and red wavelengths were marginal. Percent differences between model-estimated and measured  $L_u$  values at 1 m depth improved to 9% at 490 nm and 5.8% at 554 nm (compared to 17% and 17.2%, respectively, without allowing for small positive  $a_{t-w}(715)$ ). Similar improvement in the agreement between model and data was observed for the rest of our cruises.

### 3.3. Modeling fluorescence in the Chesapeake Bay

In addition to backscattering and absorption, fluorescence processes can significantly affect the magnitude and spectral shape of reflectance in coastal waters. For the example data set (measured [chl-*a*] of  $7.3 \text{ mg m}^{-3}$  and  $a_{CDOM}(440)$  of  $0.3 \text{ m}^{-1}$ ), model simulations underestimated  $L_u(0^-)$  in the 670–690 nm wavelength region by as much as 30–40% when chlorophyll-*a* fluorescence was neglected, compared to model results when fluorescence was included in the simulations. This underestimation of  $L_u(0^-)$  also resulted in an underestimation of  $L_w$  and  $R_{rs}$  at wavelengths close to the chlorophyll-*a* fluorescence emission maximum at 685 nm. Including chlorophyll fluorescence in our model simulations, using the Hydrolight default fluorescence efficiency of 0.02, decreased the absolute percent differences between model-estimated and measured  $L_w$  to 8% at 670 nm and 4% at 684 nm,

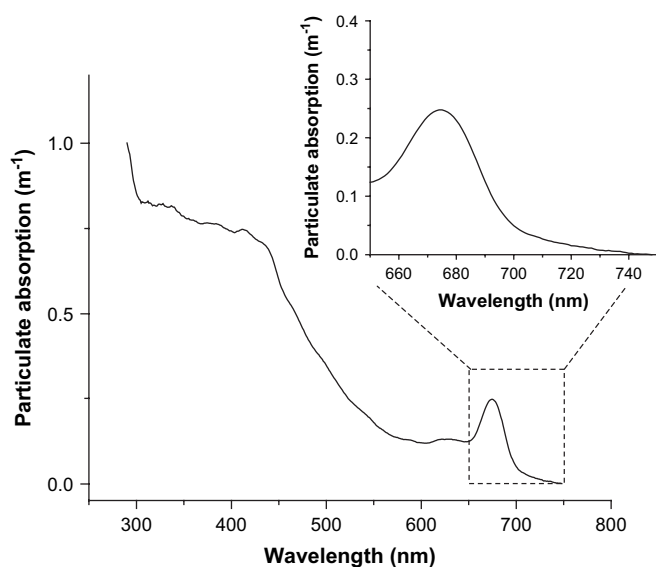


Fig. 4. Particulate absorption (sum of absorption by phytoplankton and non-algal particles) in the 290–750 nm wavelength region, measured spectrophotometrically for station PI, on 28 September 2001. The residual non-zero particulate absorption at 715 nm is shown more clearly in the inset figure.



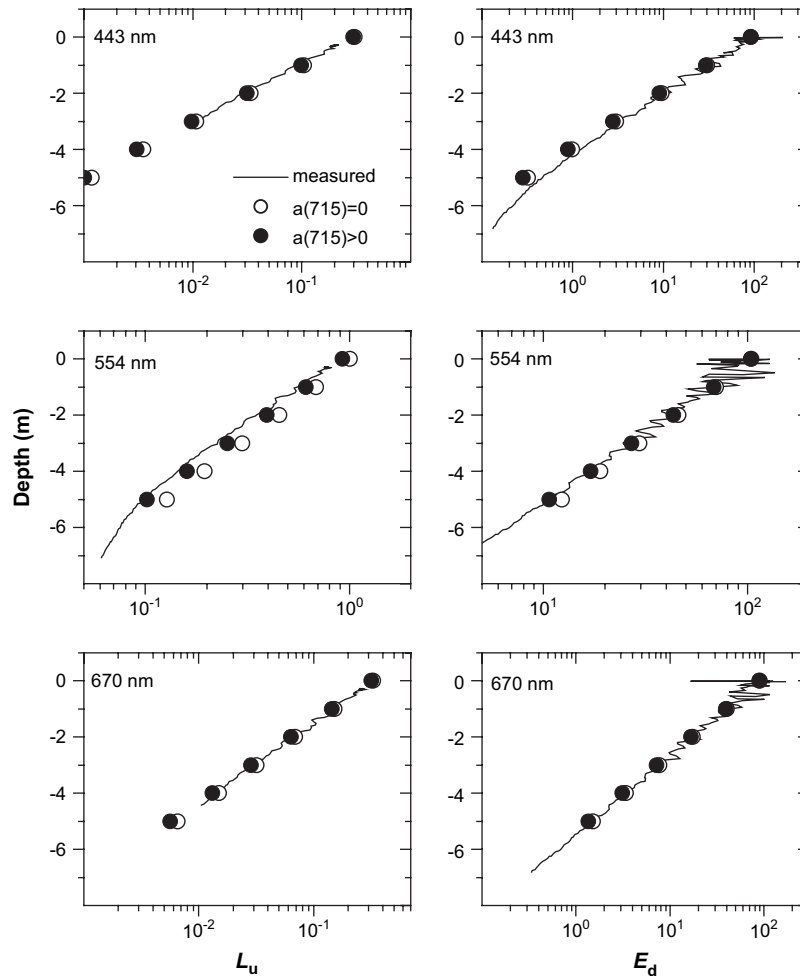


Fig. 5. (Left column) Comparison between measured (solid lines) and model-estimated  $L_u(z)$  (in  $\mu\text{W nm}^{-1} \text{cm}^{-2} \text{sr}^{-1}$ ) at 443, 554 and 670 nm, assuming  $a_{t-w}(715) = 0$  (open circles) and assuming  $a_{t-w}(715) = a_{\text{CARY}}(715)$  (filled circles).  $L_u$  values are truncated at  $0.01 \mu\text{W nm}^{-1} \text{cm}^{-2} \text{sr}^{-1}$ , due to large measurement uncertainty at low light levels. (Right column) Similarly for  $E_d(z)$  (in  $\mu\text{W nm}^{-1} \text{cm}^{-2}$ ). Data are shown for measurements performed at station PI, on 28 September 2001.

compared to 25 and 38% underestimates, respectively, when neglecting the chlorophyll fluorescence signal (Fig. 6).

The model-estimated CDOM fluorescence signal affected underwater light fields only at wavelengths shorter than 530 nm (data not shown). For the specific case studied, neglecting CDOM fluorescence in model estimations resulted in a 2–5% underestimation of  $R_{rs}$  and  $L_w$  values at the blue wavelengths, while the effect was negligible at longer wavelengths.

### 3.4. Overall radiative transfer model performance

To examine the overall radiative transfer model performance when properly accounting for the specific optical characteristics measured in the Chesapeake Bay, we performed model simulations of radiation fields for several cruises encompassing a wide range of water and boundary conditions (Table 1). Based on the foregoing results, which are summarized in Table 2, we: (1) used an FF phase function as determined by measured profiles of  $b_p/b$  spectra to account for the observed temporal and spatial variability of  $b_p/b$ , (2)

allowed for a small particulate absorption in the 715 nm wavelength region (equal to the measured  $a_{\text{CARY}}(715)$ ) when correcting AC9 absorption estimates used as input to the model, and (3) simulated chlorophyll-*a* fluorescence. For completeness, we also included fluorescence by CDOM, though neglecting CDOM fluorescence in model simulations had a relatively small effect on  $R_{rs}$  and  $L_w$  estimations.

The results of the comparisons between measured and model-estimated  $E_d(z)$  and  $L_u(z)$  are first shown for an example case of relatively turbid waters (Fig. 7 and Table 3). Model-estimated quantities were in very good agreement with measurements, especially within the first 3 m in the water column. For average values of attenuation ( $c(412) = 5.5 \text{ m}^{-1}$  and  $c(532) = 4.2 \text{ m}^{-1}$ ) measured in the Bay during our cruises, the upper 3 m correspond to optical depths ( $\zeta = c z$ ) of 16.5 and 12.5, at wavelengths 412 and 532 nm, respectively. Correspondence between model estimates and measurements in the case shown in Fig. 7 was similar to those for other days (Fig. 8). Over all model runs, average absolute percent differences between model and observed values at 1 m depth were 7.8% at 443 nm, 12.8% at 554 nm, and 8.7% at 670 nm for

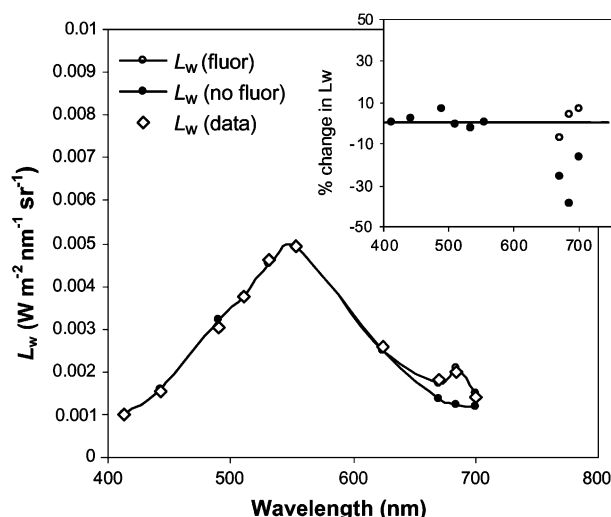


Fig. 6.  $L_w$  spectra estimated by the model, including (open circles) and neglecting (filled circles) chlorophyll-*a* fluorescence. Measured  $L_w$  are shown as open diamonds. Percent differences in  $L_w$  between measurements and model estimations are shown in the inset figure (percent differences estimated as  $(L_w(\text{model}) - L_w(\text{data}))/L_w(\text{data})$ ).

$L_u$ , and, respectively, 6.5, 5.2 and 5.9% for  $E_d$ . In general, close agreement was found for all profiles, as shown in Fig. 8 and measured by a coefficient of determination ( $R^2$ ) between model and observed values. In the upper 3 m ( $N = 356$ )  $R^2$  was 0.99 for  $E_d$  and 0.95 for  $L_u$ . For larger depths ( $N = 315$ ) estimated  $R^2$  was smaller, 0.95 and 0.92 for  $E_d$  and  $L_u$ , respectively.

Measured  $L_w$  spectra were consistently in good agreement with model results (Fig. 9, Table 4). Average absolute percent differences between data and model were 6.35% at 443 nm, 7.73% at 554 nm and 6.86% at 670 nm. The standard deviation in the percent differences ranged between 5 and 7%. The magnitude and direction of the percent differences did not show any seasonal or spatial patterns (e.g. more- versus less-turbid waters). There was not any strong tendency by the model to overestimate or underestimate  $L_w$  in the 412–670 nm wavelength region. On average, there was a slight

model overestimation of  $L_w$  in the green wavelengths, but this was smaller than the standard deviation of differences between modeled and observed  $L_w$ . Although including chlorophyll fluorescence in our model simulations considerably improved agreement between model and data, in most of the cases the model still overestimated  $L_w$  at 685 nm (average absolute difference close to 13%, Table 4).

#### 4. Discussion

Effective interpretation of ocean color in estuarine and coastal waters requires accurate modeling of bio-optical properties based on in-situ information. Therefore, successful remote retrieval of biogeochemical variables in near shore waters depends largely on the accuracy of, and consistency among, the in-situ bio-optical data used in the development, validation, and regional optimization of the applied ocean-color algorithms. It is in this sense that using radiative transfer to evaluate the validity of any modeling assumptions, and to examine the degree of closure among bio-optical quantities independently measured in the field, becomes critical for remote sensing applications (Fig. 1). In this paper, we used new, in-situ bio-optical data for the Chesapeake Bay combined with radiative transfer closure results, and found that: (1) backscattering in the Bay is highly variable in magnitude, has an average  $b_b/b$  of 0.0128, lower than that of the commonly assumed Petzold “average particle”, and can be modeled using an FF phase function as determined by measured wavelength- and depth-dependent backscattering fractions; (2) particulate matter is characterized by low, but non-zero, absorption in the 700–730 nm wavelength region, and accounting for this residual absorption is important in model simulations of  $R_{rs}$  in the green wavelengths; (3) strong sun-induced chlorophyll fluorescence considerably affects the magnitude and spectral shape of water reflectance in the red, providing a basis for satellite monitoring of [chl-*a*] in these near shore waters. The overall consistency between measured IOPs and resulting radiation fields was examined as a step towards applying data and model results to the analysis of remotely sensed ocean color in these Case 2 waters.

Backscattering in coastal waters strongly influences the magnitude of radiance leaving the water surface and eventually measured by a remote sensing instrument. Particulate backscattering in the Chesapeake Bay showed considerable variability. The backscattering fraction had an average value of 0.0128 at 530 nm, in agreement with  $b_b/b$  values reported by Sydor and Arnone (1997) for the near shore waters off Mississippi. The observed spectral shape of  $b_b/b$  is in agreement with Mobley et al. (2002), who found a weak  $b_b/b$  wavelength dependence, with a decrease in  $b_b/b$  from 442 to 555 nm by less than 24%, in the Case 2 waters offshore of New Jersey. Spatial and temporal variations in surface  $b_b$  in the Bay were strongly correlated with spatial and temporal patterns of surface non-algal particulate absorption (Tzortziou, 2004). Higher  $b_b$  values were observed consistently in the turbid water near station JT. This station is located closest to the land, is the shallowest among the four stations, and is more strongly

Table 2

Improvement of agreement between measured and model-estimated  $L_w$  as information on the specific IOPs measured at station PI (28 September 2001) is successively incorporated into the model. The final agreement between data and model demonstrates the good optical closure obtained at this study site after applying the results from our detailed measurements to properly account in the radiative transfer modeling for the observed optical characteristics

Radiative transfer modeling	Absolute % difference between model and data
1. $a_{t-w}(715) = 0$ , fluorescence included, Petzold VSF	for $L_w(554)$ : 50%
2. FF VSF with $b_b/b = 0.015$ (otherwise 1)	for $L_w(554)$ : 20%
3. FF VSF with $b_b/b(\lambda, z)$ (otherwise 1)	for $L_w(554)$ : 9%
4. $a_{t-w}(715) = a_{CARY}(715)$ (otherwise 3)	for $L_w(554)$ : 0.6%
	for $L_w(685)$ : 4%
5. Chl- <i>a</i> fluorescence not included (otherwise 4)	for $L_w(685)$ : 40%

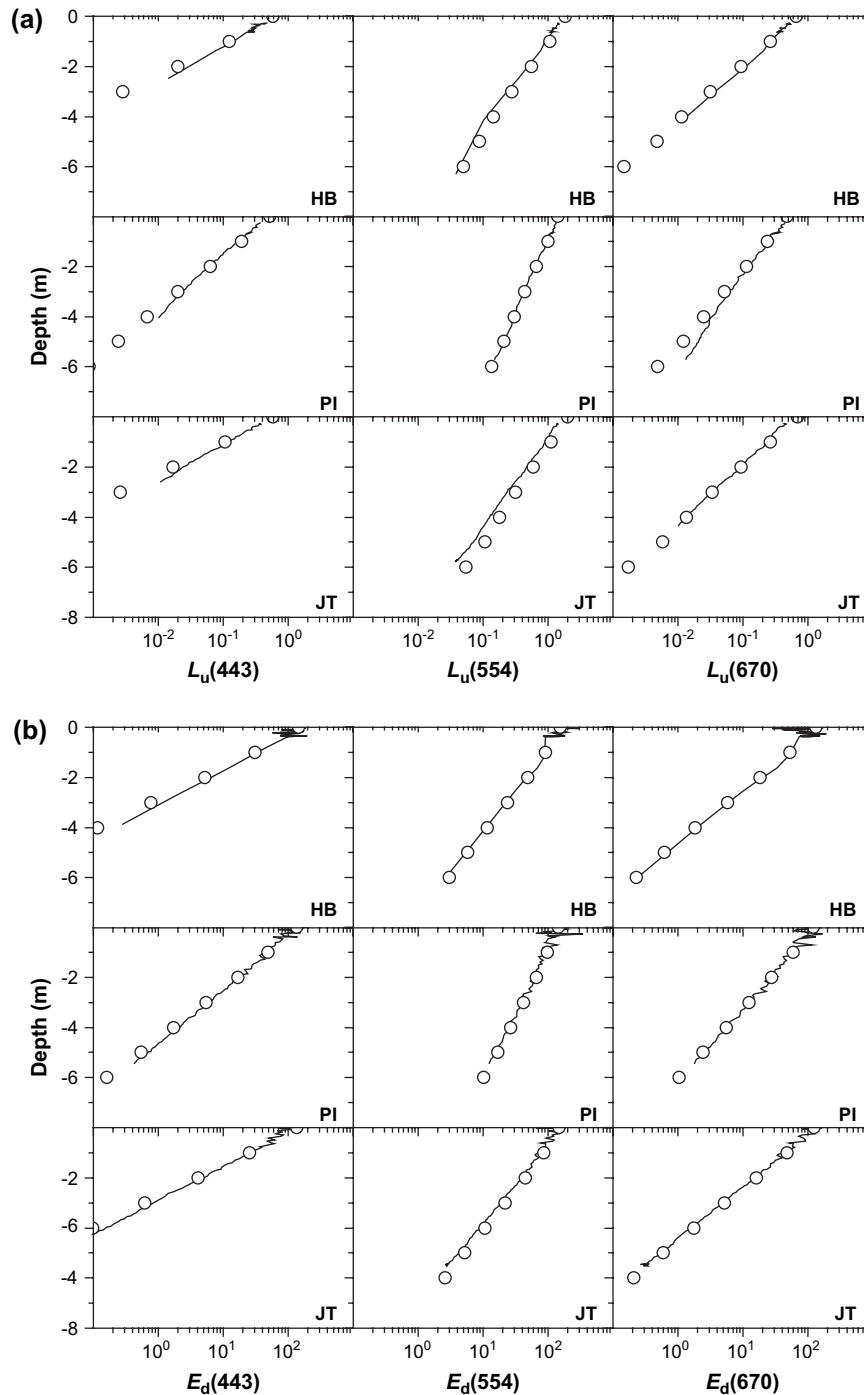


Fig. 7. (a) Model-estimated  $L_u(z)$  (in  $\mu\text{W nm}^{-1} \text{cm}^{-2} \text{sr}^{-1}$ ) (open circles), at wavelengths 443, 554, 670 nm, are compared with in-situ measurements (solid lines) performed on 22 May 2002, as an example of the degree of closure obtained during a day when highly turbid water conditions were observed in the Bay ( $L_u$  values below 0.01 are not shown here). (b) Similarly, for  $E_d(z)$  (in  $\mu\text{W nm}^{-1} \text{cm}^{-2}$ ). Percent differences between model-estimated and measured quantities at 1 m depth are given in Table 3.

influenced by bottom resuspension and shoreline erosion. These results, and the much smaller correlation found between particulate  $b_b$  and [chl-*a*], indicate that highly refractive non-algal particles, such as minerals or detrital material of relatively low water content, are the major water constituents regulating  $b_b$  variability in the region of the Chesapeake Bay we studied (Tzortziou, 2004). This information on backscattering characteristics could improve remote retrievals for the

Chesapeake Bay, through the development of new backscattering parameterizations and regional-specific algorithms that relate  $R_{rs}$  to backscattering magnitude and concentration of non-algal suspended particles.

Magnuson et al. (2004) recently examined the parameterization and validation of the semi-analytical, bio-optical Garver–Siegel–Maritorena model (i.e. GSM01, Maritorena et al., 2002) for application in the Mid-Atlantic Bight

Table 3

Percent differences in measured and model-estimated  $L_u$  and  $E_d$  (443, 554, 670 nm) at 1 m depth. Comparisons are shown for measurements representative of the most turbid waters we observed in the Bay (22 May 2002). Percent differences were estimated as:

$$\frac{L_{u(\text{model})} - L_{u(\text{data})}}{\frac{1}{2}(L_{u(\text{model})} + L_{u(\text{data})})} \times 100 \text{ (and similarly for } E_d \text{)}$$

Station	$L_u$ (wavelength in nm)			$E_d$ (wavelength in nm)		
	443	554	670	443	554	670
HB	−4.1	11.6	5.6	8.9	0.4	0.8
PI	17.4	7.4	0.6	3.5	6.4	5.5
JT	−15.5	16.4	6.7	−2.9	9	5.8

and Chesapeake Bay. According to their results, the lack of direct  $b_b$  measurements in the Bay significantly affected backscattering parameterization as well as the evaluation of the model's backscattering product. Because of the lack of backscattering data, Magnuson et al. estimated  $b_b$  from total scattering,  $b$ , assuming a constant  $b_b/b$  of 0.018 (from Petzold data). This approach resulted in an overestimation of  $b_b$  compared to the  $b_b$  product of the GSM01-CB model (i.e. the GSM01 model tuned for the Chesapeake Bay). By using a  $b_b/b$  of 0.0125, close to our mean value for surface  $b_b/b(530)$ , Magnuson et al. reduced the bias between estimated and model  $b_b$  for the Bay waters (their Fig. 11(g) and (h)).

Our radiative transfer model simulations showed that the Petzold 'average particle' assumption is usually not applicable for this region of Chesapeake Bay. As measured  $b_b/b$  in these waters had an average value of 0.0128 at 530 nm, use of the Petzold VSF with a  $b_b/b$  of 0.018 overestimated backscattered radiation compared to most observations. We obtained the best agreement between model-simulated and measured radiation fields when we modeled particulate backscattering using an FF scattering phase function as determined by measured wavelength- and depth-dependent backscattering fractions (Fig. 3, Table 2). These results are in agreement with studies by Mobley et al. (2002) for the near shore waters off the coast

of New Jersey ( $b_b/b$  within the range 0.004–0.015). The use of an FF scattering phase function constrained by measured  $b_b/b$  allowed us to incorporate information on  $b_b/b$  magnitude, spectral shape, and vertical structure into the radiative transfer model, and account for the  $b_b/b$  spatial and temporal variability observed in the Bay waters. Chang et al. (2003) performed an optical closure experiment in the near shore waters off New Jersey, in which model simulations were run using measured VSFs constant with wavelength and depth. Their average absolute percent differences between measured and model-estimated  $L_w(\lambda)$  were 20% at 443 nm, 22% at 554 nm, and 17% at 682 nm, similar to the results we obtained when using vertically and spectrally constant  $b_b/b$  (Table 2). By using measured, vertically and spectrally resolved, profiles of  $b_b/b$ , we obtained absolute percent differences between measured and model-estimated  $L_w$  smaller than 10% at all wavebands, improving optical closure in coastal waters. Therefore, detailed information on backscattering variability, including vertical and spectral resolution of backscattering processes, is necessary for radiative transfer modeling of water reflectance in the Chesapeake Bay and application of both data and model results to remote sensing algorithm development.

One common assumption when correcting in-situ AC9 data for scattering errors is that particulate absorption at 715 nm is zero (Zaneveld et al., 1994). In contrast, our measurements in the Case 2 Bay waters revealed small, non-zero particulate absorption in the wavelength region 700–730 nm. This low absorption is consistent with the gradual, exponential decrease of the non-algal particulate absorption with increasing wavelength (average  $S_{\text{nap}} = 0.011 \text{ nm}^{-1}$ ). Weak particulate absorption in the 700–730 nm was also shown by Gallegos and Neale (2002) for the Rhode River sub-estuary on the western shore of the mesohaline Chesapeake Bay, and by Tassan and Ferrari (2003), Babin and Stramski (2002), and Babin et al. (2003) for other coastal waters.

Our model simulations showed that accounting for the small particulate absorption at 715 nm when processing AC9 data (modified AC-9 correction according to Eq. (3)), further improved radiative transfer closure in the Bay waters by

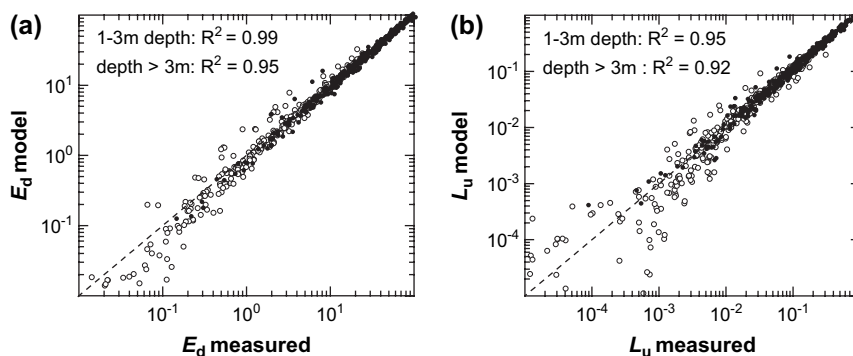


Fig. 8. Comparison between model-estimated and in-situ measured (a)  $E_d(z)$  (in  $\mu\text{W nm}^{-1} \text{cm}^{-2}$ ) and (b)  $L_u(z)$  values (in  $\mu\text{W nm}^{-1} \text{cm}^{-2} \text{sr}^{-1}$ ) at depths 0–6 m, for all cruises-stations that comparisons with the radiative transfer model were performed. Comparisons within the first 3 m are shown as dark circles ( $R^2 = 0.99$  for  $E_d$ ,  $R^2 = 0.95$  for  $L_u$ ), while comparisons for depths below 3 m are shown as open circles ( $R^2 = 0.95$  for  $E_d$ ,  $R^2 = 0.92$  for  $L_u$ ) (the 1:1 line is also shown for comparison).



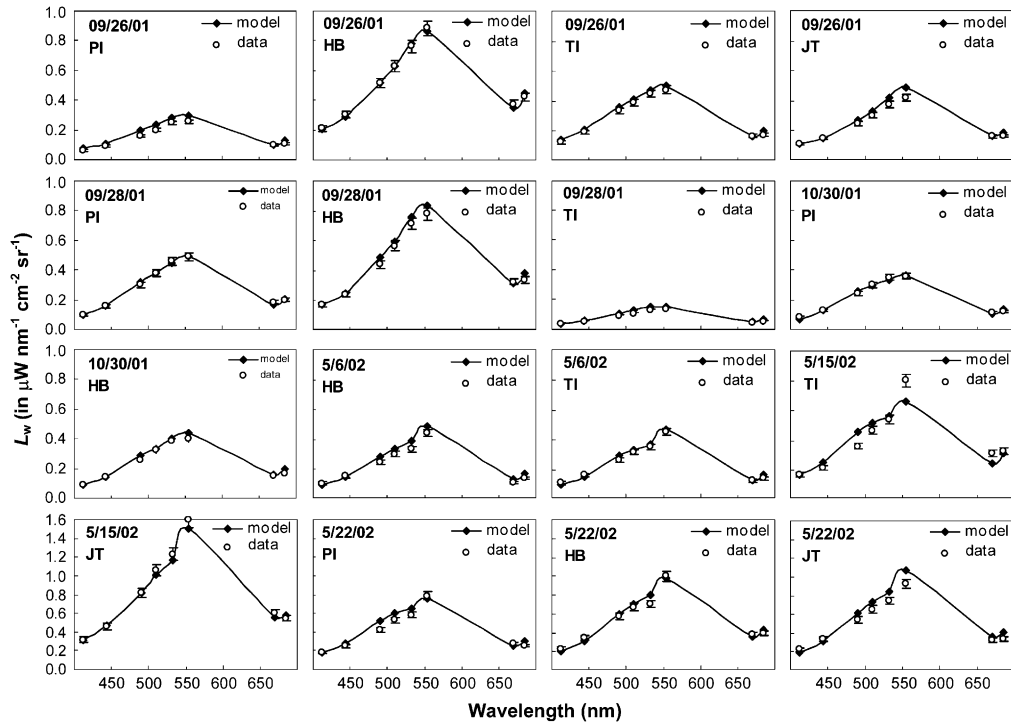


Fig. 9. Water-leaving radiances,  $L_w$ , measured in-situ (open circles) and estimated by the model (solid line, filled diamonds), for measurements performed during our cruises in the Chesapeake Bay (error bars are s.d.,  $N = 3$ ).

reducing the model's systematic overestimation of both  $E_d$  and  $L_u$ . Due to strong absorption by CDOM and non-algal particles at blue wavelengths, and water itself at red wavelengths, the effect was most noticeable at green wavelengths (i.e. 554 nm). In this wavelength region total absorption is

relatively smaller, and a small change in the absorption, equal to the weak particulate absorption at 715 nm, had a relatively larger effect on model simulations (Fig. 5). Failure to account for the small near-infrared particulate absorption when defining inputs for the radiative transfer model therefore, leads to

Table 4

Percent differences in estimated  $L_w$  values (412–685 nm) using in-situ measurements and model simulations. Percent differences were estimated as:

$$\frac{L_{w(\text{model})} - L_{w(\text{data})}}{\frac{1}{2}(L_{w(\text{model})} + L_{w(\text{data})})} \cdot 100$$

Station/date	Wavelengths (in nm)						
	412	443	490	532	554	670	685
PI, 9/26/01	−21.7	−19.4	−22.3	−13.1	−14.3	−0.3	−15.8
HB, 9/26/01	−2.7	−5.5	−0.1	2.1	−2.8	−7.4	5
TI, 9/26/01	12.9	8.5	6.6	5.1	5.1	−0.6	15
JT, 9/26/01	1.8	−0.6	7.3	12	15.2	2.1	11.3
PI, 9/28/01	0.8	1.9	6.4	−2	0.6	−7.7	4.3
HB, 9/28/01	0.6	2.9	10.3	5.5	7	−3	11.7
TI, 9/28/01	−4.7	1.1	16.6	14	12.8	8	20.3
PI, 10/30/01	−19.7	−2.1	7.2	−4.6	1.2	−3.9	14.4
HB, 10/30/01	0.6	1.5	10.2	2.8	9.5	1.4	17
HB, 5/6/02	−10	−1.7	14.1	15.3	10	18.2	21.6
TI, 5/6/02	−14	−7.5	9.5	4.8	2.3	3.1	16.3
TI, 5/15/02	−1.9	15.9	22.7	3.8	−18.6	−22.4	−4.2
JT, 5/15/02	−2.8	1.9	−0.1	−5.1	−6.1	−7	5.9
PI, 5/22/02	−2.3	11.6	18.7	10.1	−2.7	−6.5	15.5
HB, 5/22/02	−11.5	−11	3.7	12.1	−1.8	−6.6	9.1
JT, 5/22/02	−13.6	−8.5	12.1	11.8	13.7	11.5	19.9
Avg. absolute % diff (standard deviation)	7.60 (7.1)	6.35 (5.7)	10.49 (6.9)	7.76 (4.6)	7.73 (5.8)	6.86 (6.1)	12.96 (5.7)

consistent, though variable, model overestimation of  $R_{rs}$  around 554 nm. This is a key wavelength region that is being used in both empirical and semi-analytical satellite algorithms for remote chlorophyll retrievals (e.g. Carder et al., 1999; O'Reilly et al., 2000; Maritorena et al., 2002).

As fluorescence is an indicator of both the amount of chlorophyll and the rate of photosynthesis much attention has been focused on the use of remotely sensed chlorophyll fluorescence signal for inferring information on primary productivity and phytoplankton physiological state in coastal waters (e.g. Gower and Borstad, 1981; Abbott and Letelier, 1999; Huot et al., 2005). Accounting for chlorophyll fluorescence in our model simulations for the Chesapeake Bay removed large errors in modeling  $R_{rs}$  in the red wavelengths. Neglecting fluorescence for a chlorophyll concentration of  $7.3 \text{ mg m}^{-3}$  resulted in model underestimations of  $L_w$  and  $R_{rs}$  by 30–40% in the wavelength region around the chlorophyll fluorescence maximum compared to our data. Including chlorophyll fluorescence in our radiative transfer modeling of the example station considerably improved agreement between model and data reducing absolute percent differences to 4–8% (Fig. 6, Table 2). Since the ECOVSF3 measures  $b_b$  only at 450, 540 and 650 nm, model results at 685 nm are affected by uncertainties in our extrapolation of  $b_b$  constant from 650 to 685 nm (see Section 2). A tendency by the model to overestimate  $L_w$  at 685 nm could also result from an overestimate of chlorophyll fluorescence efficiency for these near-surface waters. In-situ measurements by Maritorena et al. (2000) in the Case 1, oligotrophic to eutrophic Pacific waters, showed that vertical profiles of fluorescence quantum yield were strongly structured, with maximal (5–6%) values at depth, and relatively low (1%) values closer to the surface. Similar in-situ determinations of chlorophyll fluorescence efficiency variability for the Chesapeake Bay waters would further improve model estimates of reflectance at red wavelengths. However, even with a constant fluorescence efficiency (2%) our average overestimation of  $L_w(685)$  was less than 13% over all stations (Table 4). These results suggest that remote retrieval of chlorophyll fluorescence may provide a better basis for satellite monitoring of phytoplankton in these Case 2 waters compared to  $R_{rs}$  in the blue and green where absorption is dominated by CDOM and non-algal particles.

When we applied the results from our measurements to model bio-optical processes in the Chesapeake Bay, we obtained very good closure between independently measured IOPs and radiation fields over the wide range of observed bio-optical conditions. Model  $E_d$  and  $L_u$  values, estimated from measured IOPs, were in good agreement with measurements (Figs. 7 and 8) especially within the first 3 m that, in these optically thick waters, are the most important for remote sensing. The agreement between model and data extended for over three orders of magnitude dynamic range in radiation fields. In the upper 3 m, coefficients of determination between model and observed values were 0.99 and 0.95 for  $E_d$  and  $L_u$ , respectively. Closer to the bottom, larger percent differences between model and data typically occur in such optically thick waters, since both measurements and model results have

relatively high levels of uncertainties due to very low light levels, problems with dark signal correction, and small model-input errors that propagate in the model calculations.

Although there was a wide range in the magnitude of measured  $L_w$  spectra reflecting observed variation in  $E_s$  and water IOPs,  $L_w(\lambda)$  measurements were consistently in good agreement with model results. Average absolute percent differences between measured and model-estimated  $L_w$  values were smaller than 10% in the 412–670 nm wavelength region (Fig. 9, Table 4). These percent differences were considerably smaller than those presented in the few studies of optical closure performed previously in near shore waters of similar optical complexity (e.g. Chang et al., 2003; Bulgarelli et al., 2003). The improved optical closure presented in this study was obtained after using depth and wavelength resolved measurements of  $b_b/b$ , properly correcting absorption measurements in a way that allowed a small residual particulate absorption at 715 nm, and including chlorophyll fluorescence in our model simulations. Given that our average values for  $b_b/b$  (Mobley et al., 2002; Boss et al., 2004) and  $S_{nap}$  (e.g. Roesler et al., 1989; Babin et al., 2003; Magnuson et al., 2004) were within the range of values reported in previous studies, and that our chlorophyll concentrations were not excessively high for estuaries, we expect that proper accounting for these optical characteristics would be equally important in optical modeling of other coastal and estuarine waters.

In summary, our study has shown that systematic comparisons between field observations and radiative transfer model simulations are useful for improving our knowledge of the optical characteristics (e.g.  $b_b$ ,  $b_b/b$ ,  $a$ ), as well as the importance of certain processes (e.g. CDOM and chlorophyll-*a* fluorescence), in the optically complex and biologically productive Chesapeake Bay waters. It also suggests that the radiative transfer model used in this study can be used to estimate underwater and emergent radiation fields, even in waters characterized by high optical complexity, as long as accurate input data are available and the validity of the model assumptions is examined. The demonstration of good closure between independently measured radiation fields and water IOPs using radiative transfer modeling increases confidence in the accuracy of, and consistency among the in-situ data. Obtaining closure to this degree is a critical step towards applying bio-optical data and model results to the interpretation and validation of remotely sensed ocean color, i.e. the development, parameterization, and refinement of bio-optical algorithms for effective remote retrievals of biogeochemical quantities in the Chesapeake Bay.

## Acknowledgements

Funds for this work were provided by NASA-Goddard Space Flight Center, the University of Maryland, and the Smithsonian Pre-doctoral Fellowship program. Field work on Chesapeake Bay was funded in part by the Coastal Intensive Site Network (CISNet) program of the United States Environmental Protection Agency through grant R826943-01-0. We thank K. Yee, D. Sparks, M. Mallonee and S. Benson

for assistance in the field and laboratory, and two anonymous reviewers for their constructive comments on the manuscript.

## References

- Abbott, M.R., Letelier, R.M., 1999. Chlorophyll Fluorescence (MODIS Product Number 20). MODIS Algorithm Theoretical Basis Document, ATBD-MOD-22, Version 3.
- Babin, M., Stramski, D., 2002. Light absorption by aquatic particles in the near-infrared spectral region. *Limnology and Oceanography* 47, 911–915.
- Babin, M., Stramski, D., Ferrari, G., Clauster, H., Bricaud, A., Obelensky, G., Hoepffner, N., 2003. Variations in the light absorption coefficients of phytoplankton, nonalgal particles, and dissolved organic matter in coastal waters around Europe. *Journal of Geophysical Research* 108 (C7), 3211. doi:10.1029/2001JC000882.
- Boss, E., Pegau, W.S., Lee, M., Twardowski, M.S., Shybanov, E., Korotaev, G., Baratange, F., 2004. The particulate backscattering ratio at LEO 15 and its use to study particles composition and distribution. *Journal of Geophysical Research* 109, C01014. doi:10.1029/2002JC001514.
- Bulgarelli, B., Zibordi, G., Berthon, J.F., 2003. Measured and modeled radiometric quantities in coastal waters: toward a closure. *Applied Optics* 42, 5365–5381.
- Carder, K., Stewart, R., Harvey, G., Ortner, P., 1989. Marine humic and fulvic acids: their effects on remote sensing of ocean chlorophyll. *Limnology and Oceanography* 34, 68–81.
- Carder, K.L., Chen, F.R., Lee, Z.P., Hawes, S.K., 1999. Semianalytical moderate-resolution imaging spectrometer algorithms for chlorophyll *a* and absorption with bio-optical domains based on nitrate-depletion temperatures. *Journal of Geophysical Research* 104, 5403–5421.
- Chang, G.C., Dickey, T.D., Mobley, C.D., Boss, E., Pegau, W.S., 2003. Toward closure of upwelling radiance in coastal waters. *Applied Optics* 42, 1574–1582.
- Cox, C., Munk, W., 1954. Statistics of the sea surface derived from sun glitter. *Journal of Marine Research* 13, 198–227.
- Fournier, G.R., Forand, J.L., 1994. Analytical phase function for ocean water. In: Jaffe, J.S. (Ed.), *Ocean Optics XII*, vol. 2258. SPIE – International Society for Optical Engineering, pp. 194–201.
- Gallegos, C.L., Neale, P.J., 2002. Partitioning spectral absorption in case 2 waters: discrimination of dissolved and particulate components. *Applied Optics* 41, 4220–4233.
- Garver, S.A., Siegel, D.A., 1997. Inherent optical property inversion of ocean color spectra and its biogeochemical interpretation. I. Time series from the Sargasso Sea. *Journal of Geophysical Research* 102, 18607–18625.
- Gordon, H.R., 1979. Diffuse reflectance of the ocean: the theory of its augmentation by chlorophyll *a* fluorescence at 685 nm. *Applied Optics* 18, 1161–1166.
- Gordon, H.R., Ding, K., 1992. Self-shading of in-water optical instruments. *Limnology and Oceanography* 37, 491–500.
- Gower, J.F.R., 1980. Observations of in situ fluorescence of chlorophyll *a* in Saanich Inlet. *Boundary-Layer Meteorology* 18, 235–245.
- Gower, J.F.R., Borstad, G.A., 1981. Use of in vivo fluorescence line at 685 nm for remote sensing surveys of surface chlorophyll *a*. In: Gower, J.F.R. (Ed.), *Oceanography from Space*. Plenum, NY, pp. 329–338.
- Harding Jr., L.W., Magnuson, A., 2002. Bio-optical and remote sensing observations in Chesapeake Bay. In: Fargion, G.S., McClain, C.R. (Eds.), *SIMBIOS Project 2001 Annual Report*, pp. 52–62 (NASA/TM, 2002).
- Harding Jr., L.W., Magnuson, A., Mallonee, M.E., 2005. Bio-optical and remote sensing observations in Chesapeake Bay. *Estuarine, Coastal and Shelf Science* 62, 75–94.
- Hawes, S.K., 1992. Quantum fluorescence efficiencies of marine fulvic and humic acids. Master's thesis, Dept. of Marine Sc. Univ. of South Florida, St. Petersburg, FL.
- Huot, Y., Brown, C.A., Cullen, J.J., 2005. New algorithms for MODIS sun-induced chlorophyll fluorescence and a comparison with present data products. *Limnology and Oceanography: Methods* 3, 108–130.
- Jeffrey, S.W., Humphrey, G.F., 1975. New spectrophotometric equations for determining chlorophyll *a*, *b*, *c*, and *c2* in higher plants algae and natural phytoplankton. *Biochemie und Physiologie der Pflanzen* 167, 191–194.
- Kirk, J.T.O., 1992. Monte Carlo modeling of the performance of the reflective tube absorption meter. *Applied Optics* 31, 6463–6468.
- Maffione, R.A., Dana, D.R., 1997. Instruments and methods for measuring the backward-scattering coefficient of ocean waters. *Applied Optics* 36, 6057–6067.
- Magnuson, A., Harding Jr., L.W., Mallonee, M.E., Adolf, J.E., 2004. Bio-optical model for Chesapeake Bay and the middle Atlantic bight. *Estuarine, Coastal and Shelf Science* 61, 403–424.
- Maritorena, S., Morel, A., Gentili, B., 2000. Determination of the fluorescence quantum yield by oceanic phytoplankton in their natural habitat. *Applied Optics* 39, 6725–6737.
- Maritorena, S., Siegel, D.A., Peterson, A.R., 2002. Optimization of a semi-analytical ocean color model for global-scale applications. *Applied Optics* 41, 2705–2714.
- Mitchell, G., Bricaud, A., Carder, K., Cleveland, J., Ferrari, G., Gould, R., Kahru, M., Kishino, M., Maske, H., Moisan, T., Moore, L., Nelson, N., Phinney, D., Reynolds, R., Sossik, H., Stramski, D., Tassan, S., Trees, C.C., Weidemann, A., Wieland, J., Vodacek, A., 2000. Determination of spectral absorption coefficients of particles, dissolved material and phytoplankton for discrete water samples. In: Fargion, G.S., Mueller, J.L. (Eds.), *Ocean Optics Protocols for Satellite Ocean Color Sensor Validation*, Revision 2 (NASA/TM-2000-209966, Chapter 12).
- Mobley, C.D., 1988. A Numerical Model for the Computation of Radiance Distribution in Natural Waters with Wind-roughened Surfaces, Part II; User's Guide and Code Listing. NOAA Tech. Memo ERL PMEL-81 (NTIS PB88–246871). Pacific Marine Environmental Laboratory, Seattle, Washington.
- Mobley, C.D., 1994. Light and Water: Radiative Transfer in Natural Waters. Academic Press, San Diego, CA.
- Mobley, C.D., 2002. Hydrolight Technical Note 1: How Well Does Hydrolight Simulate Wind-blown Sea Surfaces? Sequoia Scientific, Inc.
- Mobley, C.D., Sundman, L.K., 2000. Hydrolight 4.1 – Users Guide. Sequoia Scientific, Inc.
- Mobley, C.D., Sundman, L.K., Boss, E., 2002. Phase function effects on oceanic light fields. *Applied Optics* 41, 1035–1050.
- Moore, C., Twardowski, M.S., Zaneveld, J.R.V., 2000. The ECO VSF – a multi-angle scattering sensor for determination of the volume scattering function in the backward direction. In: *Proceedings from Ocean Optics XV*, October 16–20, Monaco.
- Morel, A., 1974. Optical properties of pure water and pure seawater. In: Jerlov, N.G., Steeman, E. (Eds.), *Optical Aspects of Oceanography*. Academic, London, pp. 1–24.
- Morel, A., Prieur, L., 1977. Analysis of variations in ocean color. *Limnology and Oceanography* 22, 709–722.
- Nelson, N.B., Prezelin, B.B., 1993. Calibration of an integrating sphere for determining the absorption coefficient of scattering suspensions. *Applied Optics* 32, 6710–6717.
- O'Reilly, J.E., Maritorena, S., Siegel, D., O'Brien, M.C., Toole, D., Mitchell, B.G., Kahru, M., Chavez, F.P., Strutton, P., Cota, G., Hooker, S.B., McClain, C.R., Carder, K.L., Muller-Karger, F., Harding, L., Magnuson, A., Phinney, D., Moore, G.F., Aiken, J., Arrigo, K.R., Letelier, R., Culver, M., 2000. Ocean color chlorophyll *a* algorithms for SeaWiFS, OC2, and OC4: version 4. In: Hooker, S.B., Firestone, E.R. (Eds.), *SeaWiFS Postlaunch Calibration and Validation Analyses, Part 3. SeaWiFS Postlaunch Technical Report Series*, vol. 11. NASA, Goddard Space Flight Center, Greenbelt, Maryland, pp. 9–23.
- Pegau, W.S., Gray, D., Zaneveld, J.R.V., 1997. Absorption and attenuation of visible and near-infrared light in water: dependence on temperature and salinity. *Applied Optics* 36, 6035–6046.
- Petzold, T.J., 1972. Volume Scattering Functions for Selected Ocean Waters. SIO Ref. 72-78. Scripps Inst. Of Oceanography, Visibility Laboratory, La Jolla.
- Pope, R.M., Fry, E.S., 1997. Absorption spectrum (380–700 nm) of pure water. II. Integrating measurements. *Applied Optics* 36, 8710–8723.
- Roesler, C.S., Perry, M.J., Carder, K.L., 1989. Modeling in situ phytoplankton absorption from total absorption spectra in productive inland marine waters. *Limnology and Oceanography* 34, 1510–1523.

- Satlantic, June 2002. Operation Manual for the MicroPro. Revision D. Satlantic.
- Smith, R.C., Baker, K.S., 1981. Optical properties of the clearest natural waters (200–800 nm). *Applied Optics* 20, 177–184.
- Sydor, M., Arnone, R.A., 1997. Effect of suspended particulate and dissolved organic matter on remote sensing of coastal and riverine waters. *Applied Optics* 36, 6905–6912.
- Tassan, S., 1988. The effect of dissolved “yellow substance” on the quantitative retrieval of chlorophyll and total suspended sediment concentrations from remote measurements of water colour. *International Journal of Remote Sensing* 9, 787–797.
- Tassan, S., Ferrari, G.M., 2003. Variability of light absorption by aquatic particles in the near-infrared spectral region. *Applied Optics* 42, 4802–4810.
- Tzortziou, M., 2004. Measurements and characterization of optical properties in the Chesapeake Bay estuarine waters, using in-situ measurements, MODIS satellite observations and radiative transfer modeling. PhD-dissertation, University of Maryland.
- Zaneveld, J.R.V., Kitchen, J.C., Moore, C., 1994. The scattering error correction of reflecting-tube absorption meters. In: Jaffe, J.S. (Ed.), *Ocean Optics XII*, vol. 2258. SPIE — International Society for Optical Engineering, pp. 44–55.
- Zibordi, G., Ferrari, G.M., 1995. Instrument self-shading in underwater optical measurements: experimental data. *Applied Optics* 34, 2750–2754.